Measurement-Based Blockage and Intra-Cluster Interference Analysis in mmWave Multi-Point Connectivity Networks

Rizqi Hersyandika
KU Leuven
Leuven, Belgium
rizqi.hersyandika@kuleuven.be

Juan Sanchez
Lund University
Lund, Sweden
juan.sanchez@eit.lth.se

Yang Miao
KU Leuven
Leuven, Belgium
yang.miao@kuleuven.be

Sofie Pollin
KU Leuven
Leuven, Belgium
sofie.pollin@kuleuven.be

Fredrik Tufvesson
Lund University
Lund, Sweden
fredrik.tufvesson@eit.lth.se

ABSTRACT

Millimeter-wave (mmWave) is one key enabler for high data rates in (beyond-)5G wireless communication networks. The use of directive beams and the shorter transmission range in mmWave communications make it easily obstructed or blocked by humans in dynamic real-world scenarios. Connectivity diversity, a solution to link disruption and blockage, could be achieved by deploying distributed multi-point infrastructure. To this end, a mmWave User Equipment (UE) requires a multi-reception capability. This paper investigates how different multi-point connectivity schemes, established by a set of *non-cooperative* and *cooperative* serving Base Stations (BSs), perform in the ideal Line-of-Sight (LoS) and the worst-case blocked scenarios. The results and analysis found that the impact of intra-cluster interference on spectral efficiency is much more significant than the blockage. Without any interference cancellation, regardless of LoS or blocked scenarios, adding extra serving BSs does not necessarily improve the spectral efficiency due to the dominant inter-stream interference within a cluster of services.

CCS CONCEPTS

• **Networks** → **Network performance evaluation**; **Network measurement**.

KEYWORDS

millimeter-wave (mmWave), human blockage, intra-cluster interference, multi-point connectivity, mmWave cell-free MIMO

ACM Reference Format:
Rizqi Hersyandika, Juan Sanchez, Yang Miao, Sofie Pollin, and Fredrik Tufvesson. 2022. Measurement-Based Blockage and Intra-Cluster Interference Analysis in mmWave Multi-Point Connectivity Networks. In *Emerging Topics in Wireless (EmergingWireless '22), December 9, 2022, Roma, Italy*. ACM, New York, NY, USA, 6 pages. https://doi.org/10.1145/3565474.3569071

EmergingWireless '22, December 9, 2022, Roma, Italy

ACM ISBN 978-1-4503-9934-0/22/12…$15.00
https://doi.org/10.1145/3565474.3569071

1 INTRODUCTION

Millimeter-Wave (mmWave) bands are preferred in (beyond-)5G wireless communication networks, as their abundant bandwidth support high data rate communication [1]. Due to high free-space propagation loss in these bands, directive beams are used to compensate for such loss. Consequently, a mmWave link can be easily blocked by an object or human, resulting in a significant attenuation.

In the sub-6 GHz band, connectivity diversity achieved by multi-point connectivity aims to improve spectral efficiency. One form of connectivity diversity is cell-free massive Multiple-Input-Multiple-Output (MIMO), where multiple coordinated and distributed Base Stations (BSs) serve a smaller number of User Equipment (UE) simultaneously in the same time-frequency domain [2]. It requires a large number of cooperative BSs orchestrated by a Central Processing Unit (CPU) to be densely deployed.

Going up to mmWave frequencies, multi-point and/or multi-beam could alleviate the blockage problem of mmWave links and guarantee link reliability. Distinct mmWave features such as directive beams, smaller transmission ranges and being easily influenced by blockers make the implementation of multi-point connectivity in this band require further investigation. In [3, 4], it is demonstrated that using cooperative BSs can improve the coverage and link reliability against blockage in mmWave cellular networks. In [5], the use of cooperative multi-point BSs for enhancing link reliability and suppressing interference in mmWave cellular network has been studied using measured data where the simultaneous transmission/reception is limited to up to three reception beams with limited combining schemes. Several studies on mmWave cell-free have been performed. In [6, 7], a theoretical performance analysis of mmWave cell-free MIMO is discussed. User association and beam alignment in mmWave cell-free have been studied in [8, 9], while the mobility issue in mmWave cell-free has been tackled in [10].

Although the previous studies have demonstrated the advantage of spectral efficiency brought by mmWave cell-free MIMO, *the measurement-based analysis on the impact of blockage and intra-cluster interference in mmWave multi-point connectivity, in particular the mmWave cell-free MIMO, is missing*. Without doing this, we could not conclude the benefit of mmWave cell-free MIMO when subject to intense blockage and interference. This paper investigates the capacity performances of mmWave cell-free MIMO and

compares it with a non-cooperative multiple-points of Single-Input-Single-Output (M-SISO) approach, considering the multi-reception ability of a mmWave user through a measurement campaign.

The contributions of this work are as follows:

- We leverage our mmWave and massive MIMO testbed to create a cluster of mmWave multi-point networks with different multi-point connectivity schemes, in which a set of BSs serves a UE with multiple RF chains simultaneously in the cooperative and non-cooperative way. The scenario where a set of cooperative BSs serve a UE represents a cluster of mmWave cell-free MIMO networks.
- In addition to evaluating multi-point connectivity in ideal Line-of-Sight (LoS) scenarios, we also investigate the network performance with the presence of multiple blockers mimicking the realistic mmWave scenario where the blockage is one challenging but common issue. Attenuation per link due to the blockage is analyzed, and the advantage of having multiple receiving beams at UE is demonstrated.
- A noticeable insight from our measurement results is that having multiple serving BSs does not necessarily bring enhanced spectral efficiency since inter-beam (intra - cluster) interference is still dominant in practice. We observed that the intra-cluster interference impact on the capacity performance is more significant than the blockage.

To the best of our knowledge, it is the first measurement-based study on the performance of mmWave cell-free MIMO networks under realistic blockage scenarios. From the measurement results, we analyze both human blockage and intra-cluster interference impacts on the spectral efficiency performance of different mmWave multi-point connectivity schemes, providing instructive insight to the wireless communication community reaching beyond mmWave frequencies.

2 MULTI-POINT CONNECTIVITY SCHEMES

In single-point connectivity, each UE only establishes a connection with one serving BS, which is not reliable for mmWave communications in dynamic environments as the directive mmWave link is highly vulnerable to blockage by, e.g., humans or vehicles. Therefore, mmWave multi-point connectivity has been proposed for enhancing reliability and coverage [5]. To this end, multiple BSs should be densely deployed to cover the area to ensure link availability.

Fig. 1 illustrates two mmWave multi-point connectivity schemes working in non-cooperative and cooperative ways. To this end, a UE is equipped with multiple RF chains enabling multi-reception from a set of serving BSs. The illustration only shows one cluster serving one UE, whereas, in reality, multiple clusters exist, and each BS has a multiple-transmission capability to serve multiple UEs simultaneously.

2.1 Non-cooperative M-SISO

In the cellular system, a non-cooperative scheme in which there is no cooperation among cells (i.e., BSs do not share channel information) has been studied [11]. For the non-cooperative multi-point connectivity scheme, we consider that a set of spatially distributed

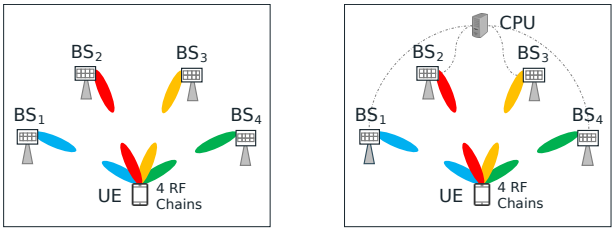

(a) Non-cooperative M-SISO **(b) Cooperative MIMO**

Figure 1: Illustration of mmWave multi-point connectivity schemes

serving BSs sends multiple SISO streams to a UE without cooperation. A cluster consists of L serving BSs and one UE, where each BS serves the UE with one beam. Reciprocally, the UE receives from each BS with an associated beam. That is, L receiving beams, supported by L RF chains, are used at the UE side for directional reception. The received downlink signal from BS_l at the UE, $\hat{\mathbf{y}}_l \in \mathbb{C}^{L\times 1}$, can be expressed as:

$$\hat{\mathbf{y}}_l = \sqrt{p_l}\hat{\mathbf{h}}_l \hat{s}_l + n, \tag{1}$$

where p_l is the transmit power at BS_l, $\hat{\mathbf{h}}_l \in \mathbb{C}^{L\times 1}$ is the channel transfer function between BS_l and the UE, including the antenna gain at both sides, $\hat{s}_l$ is the transmitted information, and n is the noise at the UE.

Since the subset of serving BSs are not cooperating, any signal received by each UE's beam other than that from the intended associated BS causes interference. Therefore, each UE's RF chain computes the signal-to-interference-and-noise ratio (SINR) individually without any combining scheme, and thus, the UE treats the transmission as multiple SISO links. The downlink SINR of transmission from BS_l to the UE for this scheme is calculated as follows:

$$SINR_l^{DL} = \frac{p_l|\hat{\mathbf{h}}_l|^2}{\sum_{j<l} p_j|\hat{\mathbf{h}}_j|^2 + n^2}, \tag{2}$$

where $\hat{\mathbf{h}}_j \in \mathbb{C}^{L\times 1}$ represents the undesired signal from other serving BSs causing intra-cluster interference. Since only one UE is considered, inter-cluster interference is not taken into account. The aggregated downlink spectral efficiency of the UE is then calculated as follows:

$$SE^{DL} = \sum_{l=1}^{\tilde{L}} \log_2(1 + SINR_l^{DL}). \tag{3}$$

2.2 Cooperative (Cell-Free) MIMO

In this scheme, a set of spatially distributed cooperative BSs serves the UE at the same time-frequency domain. Each serving BS shares the channel information of the UE collected during the channel estimation period. The channel information from all serving BSs is gathered by the CPU through fronthaul links. The CPU combines all of them to design a precoding vector for each serving BS to transmit information to the UE, creating a cell-free MIMO multi-point scenario. During the channel estimation period, all L serving BSs estimate their channels with the UE, denoted as $\hat{\mathbf{h}}_l \in \mathbb{C}^{L\times 1}$,

and the CPU combines all estimated channels between the set of serving BSs with UE as $\hat{\mathbf{H}} = [\hat{\mathbf{h}}_1, \dots, \hat{\mathbf{h}}_L]$ where $\hat{\mathbf{H}} \in \mathbb{C}^{L \times L}$.

We consider the Maximum Ratio (MR) and the Zero Forcing (ZF) precoding schemes for the joint processing of the cooperating multi-point BSs. The combined channel estimation $\hat{\mathbf{H}}$ is used to calculate the combining vector. The combining vector of MR is represented as follows [12]:

$$\mathbf{V}^{\mathrm{MR}} = \hat{\mathbf{H}} \in \mathbb{C}^{L \times L}, \tag{4}$$

while the combining vector of ZF is represented as follows:

$$\mathbf{V}^{\mathrm{ZF}} = \hat{\mathbf{H}} \left(\hat{\mathbf{H}}\right)^{\mathrm{H}} \hat{\mathbf{H}}\right)^{-1} \in \mathbb{C}^{L \times L}, \tag{5}$$

in which $\mathbf{V} = [\mathbf{v}_1, \dots, \mathbf{v}_l]$. The precoding vector of the UE is calculated as follows:

$$\mathbf{w}_l = \frac{\mathbf{v}_l}{\|\mathbf{v}_l\|}, \tag{6}$$

where $\mathbf{w}_l \in \mathbb{C}^{L \times 1}$ is normalized and $\mathbf{W} = [\mathbf{w}_1, \dots, \mathbf{w}_l] \in \mathbb{C}^{L \times L}$ is the precoding matrix. Since we consider channel reciprocity in Time Division Duplex (TDD), the precoded signal transmitted by BS_l to the UE becomes:

$$\hat{x_l} = \mathbf{w}_l \hat{s_l}, \tag{7}$$

thus the downlink received signal at the UE becomes:

$$\hat{\mathbf{y}}_l = \sqrt{p_l}\hat{\mathbf{h}}_l \cdot \mathbf{w}_l \hat{s}_l + n. \tag{8}$$

The downlink SINR of transmission from BS_l to the UE is calculated as follows:

$$SINR_l^{DL} = \frac{p_l |\mathbf{w}_l^{\mathrm{H}} \hat{\mathbf{h}}_l|^2}{\sum_{j<l} p_j |\mathbf{w}_j^{\mathrm{H}} \hat{\mathbf{h}}_j|^2 + n^2}. \tag{9}$$

Unlike in the non-cooperative M-SISO scheme, in cooperative MIMO, the precoding vector $\mathbf{W}$ is aimed at suppressing the intra-cluster interference from other serving BSs, especially in the ZF scheme. The aggregated spectral efficiency per user is calculated using (3).

3 MEASUREMENT CAMPAIGN

3.1 The mmWave MIMO testbed

Our mmWave MIMO testbed consists of a pair of Butler Matrix units, a mmWave front-end operating in the frequency range of 25 - 30 GHz, and multiple USRPs. A Butler Matrix unit can either transmit or receive 16 orthogonal beams where the pattern of the beams depends on frequency [13]. The beam pattern of the Butler Matrix at 26.0 GHz is depicted in Fig. 2, in which the beams at the centre have a narrower beamwidth and higher gain compared to the beams at the edge. The gain differences between the strongest and weakest beams can reach up to 20 dB.

The Tx USRP transmitting intermediate frequency f_{IF} of 2.4 GHz with 20 MHz bandwidth is used to generate the mmWave signal f_{RF} at 26.0 GHz. The f_{IF} is inputted to an input port of the Tx Butler Matrix, and ERASynth+ RF Signal Generator operating at f_{LO} = 11.8 GHz is connected to the Local Oscillator (LO) port of the Butler Matrix. The up/down conversion taking place in a Butler Matrix unit follows [14]: $f_{RF} = 2f_{LO} + f_{IF}$.

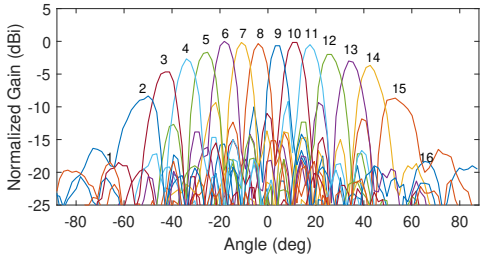

Figure 2: Beam pattern of Butler Matrix at 26 GHz

In the Rx Butler Matrix, all 16 beams receive the signals coming from different directions of all transmitters. All available ports of the Rx Butler Matrix are connected to the 16 input ports of Rx USRPs, and the LO port of the Butler Matrix is connected to the signal generator. The signal generator is synchronized for both Tx and Rx Butler Matrix. The additional Rx gain of 31.5 dB is added to the Rx USRPs.

All USRPs run LabView Communications MIMO Application Framework [15]. Pulse Per Second (PPS) and 10 MHz clock reference signals are used to synchronize the Tx and Rx USRPs. The framework has a TDD signal frame structure with OFDM symbols where the uplink pilot is used to estimate the channel. The measurement parameters are shown in Table 1.

3.2 Measurement scenario

The measurement scenario mimics a cluster of the user-centric network in which a UE is served by multiple BSs simultaneously. We consider up to eight distributed BSs where the different colour of the beam indicates different serving BS, as is depicted in Fig. 3. The Tx Butler Matrix acts as a serving BS that performs downlink transmission to the Rx Butler Matrix, acting as a UE. The measurements are conducted in an indoor environment of 11×6.5 m^2. UE is located in the far field of all serving BSs; the nearest and the farthest distance between UE and serving BSs are 2.4 m and 3.4 m, respectively. The height of the UE and the BSs is 90 cm from the ground. The same heights for UE and BS are chosen because the Butler Matrix beams are fixed and separated in 2D. Despite this, it mimics the real-world scenario because the BS beam would steer to the UE in any case.

The scenario implementation challenge is that only one pair of Tx and Rx Butler Matrix units is available, making it impossible to realize simultaneous transmissions from eight different BSs. Nevertheless, we aim to capture the stationary scenario in coherent

Table 1: Measurement parameters

Parameter	Value
BS transmit power (p_l)	0.1 mW
Operating frequency (f_{RF})	26.0 GHz
Bandwidth	20 MHz
Additional Rx gain	31.5 dB
Noise (n^2)	-93.85 dBm
Distance of UE - BSs	2.4 - 3.4 m
Height of UE - BSs	90 cm

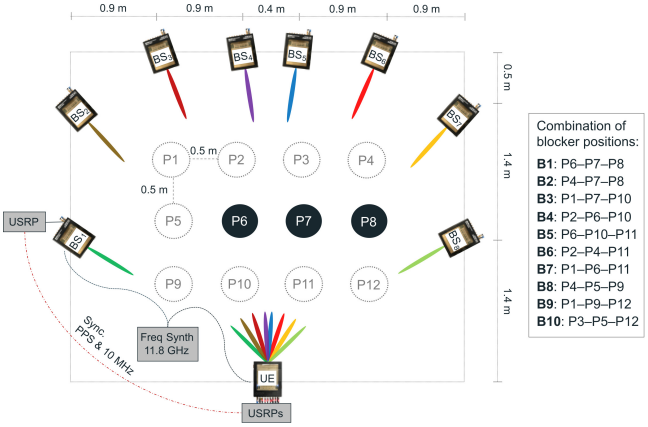

Figure 3: Measurement setup and blockage scenario

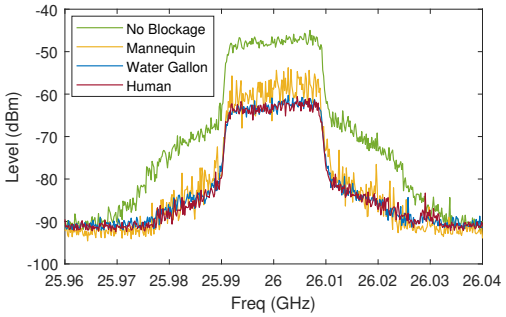

Figure 4: Attenuation of various objects

snapshots (time samples) and sequentially measure the channel for eight different BS positions and blocker positions. The position of UE and eight serving BSs is illustrated in Fig. 3. In each measurement, 100 symbols are captured, in which a symbol duration contains 100 complex channel state information samples of 100 subcarriers per receive antenna. UE measures the channel using 8 out of 16 Rx available beams in which Rx beams: 2, 4, 6, 8, 9, 11, 13 and 15, as indicated in Fig. 2, are selected at the UE. The selection of those beams is based on the physical beam alignment with all serving BSs. We capture the complex channel information for each BS position and combine the channel information of all serving BSs through post-processing. This way, the intra-cluster interference from other serving BSs is also captured.

We also aim to capture the human blockage impact since it significantly affects the performance of 5G mmWave communications in the 26 GHz band [16]. To capture the effect of multiple blockers, we used objects representing multiple human blockers in the field of view of the mmWave BSs-UE cluster. In each measurement run, three blockers are placed in three different points out of twelve possible points (P1 to P12). Ten different position combinations (B1 to B10) are realized to represent the multi-blockers' randomness, as depicted in Fig. 3.

3.3 Human blockage emulation

To ensure the measurement's reproducibility and repeatability, and to avoid ethical concerns, we do not use real human as a blocker. Instead, we use objects with similar attenuation properties to emulate the human body as a blocker. Several papers have studied the emulation of human blockers using objects such as phantom and water-filled pipes [17, 18].

We conducted preliminary measurements with different objects, such as a mannequin made of fibre and a 19 L gallon with a diameter of 27 cm filled with water, to find one that can represent the human blockage between the mmWave link. The received signal level is measured using a spectrum analyzer with the results shown in Fig. 4. From the results, attenuation caused by the presence of the human body is 14.7 dB, approaching the attenuation results obtained by [19] which is up to 13.9 dB at 26 GHz. The received signal level caused by the water gallon is similar to that caused by the actual human body, indicating similar attenuation properties between them. Meanwhile, the fibre mannequin causes less attenuation compared to the human body. Therefore, the gallon filled with water is chosen to replace the human body as a blocker for enabling repeatable blockage measurements.

4 NUMERICAL ANALYSIS

4.1 Attenuation per mmWave link analysis

Multi-blockers' presence results in a lower received power compared to the non-blocked scenario. Each link is affected differently by the blockage, as can be seen in Fig. 5. The figure presents the different consequences on link performance resulting from the ten different positions B1, B2, $\cdots$, B10 of the three blockers. The received power levels from the eight beam pairs between UE and the BSs are presented for each blocked scenario. One notable beam characteristic of the Butler Matrix is the lower array gain for beams at the edge of the field of view, as was shown in Fig. 2. It results in a lower received power at UE from BS_1 and BS_8, even in a free space scenario. Blocking these beam pairs influences the received power level significantly, as shown in Scenario B8 and B9 in Fig. 5, where the BS_1-UE link is blocked.

The most significant link power degradation due to blockage is observed in Scenario B5, where four beams are affected by two blockers standing close to the UE (P10 and P11 in Fig. 3). Meanwhile, the least degradation is observed in Scenario B10, verifying that the performance degradation caused by human blockage can vary a lot depending on the positions of the blockers. The CDF of the received power level for the free space and all the blocked scenarios is shown in Fig. 6. It shows that almost 20% of the power levels in blocked scenarios are below the minimum power level in the free-space scenario. By having multi-point connections with spatially distributed BSs, one or several beam pairs will not be affected by the blockage, as shown in Fig. 5.

4.2 Spectral efficiency analysis

The number of serving BSs is proportional to the aggregated spectral efficiency. However, increasing the number of serving BSs leads to higher intra-cluster interference, according to (2) and (9). Despite using a narrow beam for communication, the multi-point connectivity still experiences intra-cluster interference, affecting the SINR performance. The signal power leakage due to the imperfect beam

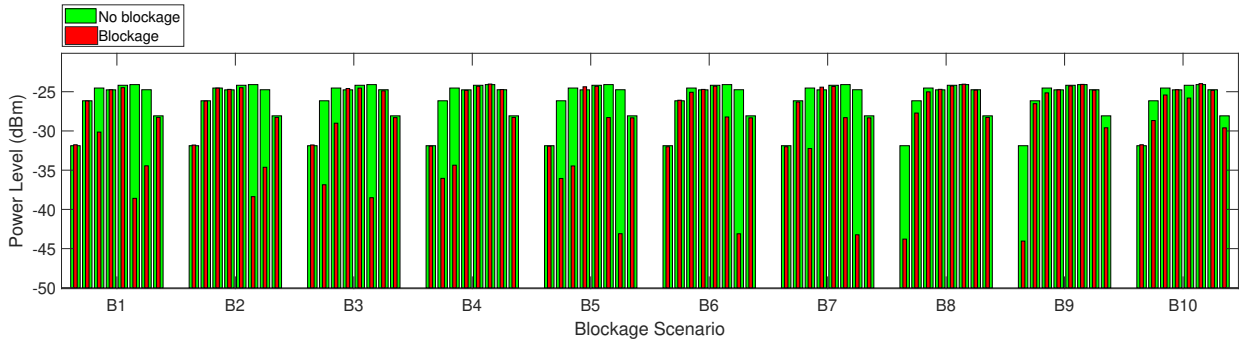

Figure 5: Attenuation per mmWave link

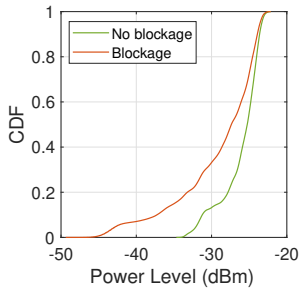

Figure 6: Rx power level

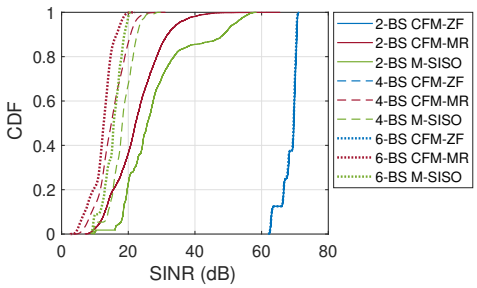

Figure 7: Intra-cluster interference

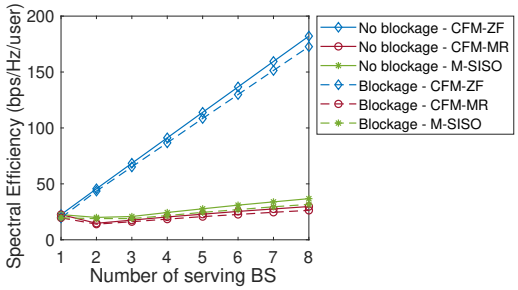

Figure 8: Spectral efficiency

pattern of the Butler Matrix, as shown in Fig. 2, as well as the reflection from the environment, are the main factors contributing to the intra-cluster interference. Fig. 7 describes how the increase in the number of serving BSs affects intra-cluster interference under different multi-point connectivity schemes. For the same number of serving BSs, the SINR of Cell-Free MIMO with Zero Forcing precoding (CFM-ZF) scheme is significantly higher than both non-cooperative M-SISO and Cell-Free MIMO with Maximum Ratio precoding (CFM-MR) schemes due to the optimal combining vector of ZF that cancels out the noise and interference. Besides, adding additional serving BSs in M-SISO and CFM-MR schemes significantly reduces the SINR because of the increasing of intra-cluster interference. However, it's not the case with the CFM-ZF scheme; regardless of the number of serving BSs, the noise and interference suppression capability is stable.

Fig. 8 shows the comparison of the spectral efficiency for the mentioned multi-point connectivity schemes. The spectral efficiency of single-point connectivity is indicated by one serving BS. In the M-SISO and CFM-MR schemes, having two serving BSs decreases the spectral efficiency as the interference increases. After adding a certain number of serving BSs (i.e. four and five for M-SISO and CFM-MR, respectively), the spectral efficiency starts matching the single-point connectivity. It indicates that these two schemes are inefficient, considering the number of serving BS required to level up with the spectral efficiency of the single-point connectivity scheme. On the contrary, with the CFM-ZF scheme, the spectral efficiency grows linearly with the increasing number of serving BSs. CFM-ZF significantly outperforms other multi-point connectivity schemes regarding spectral efficiency, primarily when more BSs are used, due to its better intra-cluster interference suppression capability than others.

The blockage slightly reduces the spectral efficiency in all schemes. However, the spectral efficiency gap between CFM-ZF and two other schemes is significant. Having only two serving BSs in CFM-ZF already outperforms the spectral efficiency performance of eight serving BSs without interference cancellation. It shows that the impact of intra-cluster interference is much more significant than the blockage.

5 CONCLUSION

This paper presents a measurement-based blockage and intra-cell interference analysis on the performance of different mmWave multi-point connectivity schemes under the ideal LoS and the blocked scenarios. The multi-point connectivity schemes are evaluated in a cluster with multiple BSs serving one UE. One scheme with the cooperation between BSs represents the mmWave cell-free MIMO networks. From the numerical analysis, the cooperative (cell-free) MIMO with the ZF scheme achieves significantly higher spectral efficiency than the other schemes, regardless of the blocked or free-space scenario. The advantage of having multi-point connectivity under blocked circumstances is also demonstrated. One noticeable insight is that the intra-cluster interference impact on the capacity performance is much more significant than the blockage. Thus, a scheme with better interference cancellation is crucial for mmWave

multi-point connectivity networks. We will consider adding multiple users to analyze the impact of inter-cluster interference for future work.

ACKNOWLEDGMENTS

This work has received funding from the EU-H2020 MSCA-ITN-2019 under grant agreement No. 861222 (MINTS project).

REFERENCES

[1] Theodore S. Rappaport, Shu Sun, Rimma Mayzus, Hang Zhao, Yaniv Azar, Kevin Wang, George N. Wong, Jocelyn K. Schulz, Mathew Samimi, and Felix Gutierrez. Millimeter Wave Mobile Communications for 5G Cellular: It Will Work! *IEEE Access*, 2013. doi: 10.1109/ACCESS.2013.2260813.

[2] Hien Quoc Ngo, Alexei Ashikhmin, Hong Yang, Erik G. Larsson, and Thomas L. Marzetta. Cell-Free Massive MIMO Versus Small Cells. *IEEE Transactions on Wireless Communications*, 2017. doi: 10.1109/TWC.2017.2655515.

[3] Diana Maamari, Natasha Devroye, and Daniela Tuninetti. Coverage in mmWave Cellular Networks With Base Station Co-Operation. *IEEE Transactions on Wireless Communications*, 2016. doi: 10.1109/TWC.2016.2514347.

[4] Dileep Kumar, Jarkko Kaleva, and Antti Tolli. Blockage-Aware Reliable mmWave Access via Coordinated Multi-Point Connectivity. *IEEE Transactions on Wireless Communications*, 2021. doi: 10.1109/twc.2021.3057227.

[5] George R. MacCartney and Theodore S. Rappaport. Millimeter-Wave Base Station Diversity for 5G Coordinated Multipoint (CoMP) Applications. *IEEE Transactions on Wireless Communications*, 2019. doi: 10.1109/TWC.2019.2913414.

[6] Guillem Femenias and Felip Riera-Palou. Cell-Free Millimeter-Wave Massive MIMO Systems With Limited Fronthaul Capacity. *IEEE Access*, 2019. doi: 10.1109/ACCESS.2019.2908688.

[7] Mario Alonzo and Stefano Buzzi. Cell-free and user-centric massive MIMO at millimeter wave frequencies. In *2017 IEEE 28th Annual International Symposium on Personal, Indoor, and Mobile Radio Communications*, 2017. doi: 10.1109/PIMRC.2017.8292302.

[8] Rizqi Hersyandika, Qing Wang, and Sofie Pollin. Association in Dense Cell-Free mmWave Networks. In *2021 IEEE International Conference on Communications*, 2021. doi: 10.1109/ICC42927.2021.9500294.

[9] Stefano Buzzi, Carmen D'Andrea, Maria Fresia, and Xiaofeng Wu. Beam Alignment in mmWave User-Centric Cell-Free Massive MIMO Systems. In *2021 IEEE Global Communications Conference*, 2021. doi: 10.1109/GLOBECOM46510.2021.9685521.

[10] Carmen D'Andrea, Giovanni Interdonato, and Stefano Buzzi. User-centric Handover in mmWave Cell-Free Massive MIMO with User Mobility. In *2021 29th European Signal Processing Conference*, 2021. doi: 10.23919/EUSIPCO54536.2021.9616361.

[11] Thomas L. Marzetta. Noncooperative Cellular Wireless with Unlimited Numbers of Base Station Antennas. *IEEE Transactions on Wireless Communications*, 2010. doi: 10.1109/TWC.2010.092810.091092.

[12] Emil Björnson, Jakob Hoydis, and Luca Sanguinetti. Massive MIMO Networks. *IEEE Communications Magazine*, 2017. doi: 10.1561/2000000093.Simulation.

[13] Xiaozhou Wang, Martin Laabs, Dirk Plettemeier, Keishi Kosaka, and Yasuhiko Matsunaga. 28 GHz Multi-Beam Antenna Array based on Wideband High-dimension 16x16 Butler Matrix. In *2019 13th European Conference on Antennas and Propagation*, 2019.

[14] Achiel Colpaert, Evgenii Vinogradov, and Sofie Pollin. Fixed mmWave Multi-User MIMO: Performance Analysis and Proof-of-Concept Architecture. In *2020 IEEE 91st Vehicular Technology Conference*, 2020. doi: 10.1109/VTC2020-Spring48590.2020.9128958.

[15] National Instruments. 5G Massive MIMO Testbed: From Theory to Reality, 2022. URL https://www.ni.com/fr-be/innovations/white-papers/14/5g-massive-mimo-testbed--from-theory-to-reality--.html.

[16] Hamidou Dembele, Marie LE Bot, François Gallee, and Patrice Pajusco. Impact of Human Blockage on 5G Communication System in the 26 GHz Band. In *15th European Conference on Antennas and Propagation*, 2021. doi: 10.23919/EuCAP51087.2021.9411015.

[17] Carl Gustafson and Fredrik Tufvesson. Characterization of 60 GHz shadowing by human bodies and simple phantoms. In *6th European Conference on Antennas and Propagation*, 2012. doi: 10.1109/EuCAP.2012.6206265.

[18] Maryam Faizi Khajeim, Gholamreza Moradi, Reza Sarraf Shirazi, and Shuai Zhang. A Body-Blockage Analysis and Comparison Between Humans and a Full-Body Phantom: Using Measurements at 28 GHz. *IEEE Antennas and Propagation Magazine*, 2021. doi: 10.1109/MAP.2021.3089988.

[19] Xiongwen Zhao, Qi Wang, Shu Li, Suiyan Geng, Mengjun Wang, Shaohui Sun, and Zhu Wen. Attenuation by Human Bodies at 26- and 39.5-GHz Millimeter Wavebands. *IEEE Antennas and Wireless Propagation Letters*, 2017. doi: 10.1109/LAWP.2016.2629023.